Is Soft Carbon a More Suitable Match for SiO_x in Li-Ion Battery Anodes?

Qing Sun[1,4,5,&], Guifang Zeng[2,3,&], Shang Wang[3,*], Marc Botifoll[6], Hao Wang[7], Hongbin Liu[1], Deping Li[1], Fengjun Ji[1], Yanhong Tian[3,*], Jordi Arbiol[6,8], Andreu Cabot[2,8,*], Lijie Ci[1,*]

[1] State Key Laboratory of Advanced Welding and Joining, School of Materials Science and Engineering, Harbin Institute of Technology (Shenzhen), Shenzhen 518055, China

[2] Catalonia Institute for Energy Research – IREC, Sant Adrià de Besòs, Barcelona 08930, Spain

[3] Department of Electronic and Biomedical Engineering, Universitat de Barcelona, Barcelona 08028, Spain

[4] State Key Laboratory of Advanced Welding and Joining, Harbin Institute of Technology, Harbin 150001, China

[5] Research Center for Carbon Nanomaterials, Key Laboratory for Liquid-Solid Structural Evolution & Processing of Materials (Ministry of Education), School of Materials Science and Engineering, Shandong University, Jinan 250061, China

[6] Catalan Institute of Nanoscience and Nanotechnology (ICN2), CSIC and BIST, Campus UAB, Bellaterra, Barcelona 08193, Spain

[7] Land Transport Authority of Singapore, Singapore 179102, Singapore

[8] ICREA Pg. Lluis Companys, Barcelona 08010, Spain

[&] These authors contributed equally to this work

* Corresponding authors

E-mail addresses:

ShangWang (wangshang@hit.edu.cn),

Yanhong Tian (tianyh@hit.edu.cn),

Andreu Cabot (acabot@irec.cat),

Lijie Ci (cilijie@hit.edu.cn)

Keywords: lithium-ion batteries; SiO_x/C anode; working potential match; operando X-ray diffraction

Abstract

Silicon oxide (SiO_x), inheriting the high-capacity characteristic of silicon-based materials but possessing superior cycling stability, is a promising anode material for next-generation Li-ion batteries. SiO_x is typically applied in combination with graphite (Gr), but the limited cycling durability of the SiO_x/Gr composites curtails large-scale applications. In this work, we demonstrate that this limited durability is in part related to the presence of a bidirectional diffusion at the SiO_x/Gr interface, which is driven by their intrinsic working potential differences and the concentration gradients. When Li on the Li-rich surface of SiO_x is captured by Gr, the SiO_x surface shrinks, hindering further lithiation. We further demonstrate that the use of soft carbon (SC) instead of Gr can prevent such instability. The higher working potential of SC avoids bidirectional diffusion and surface compression thus allowing further lithiation. In this scenario, the evolution of the Li concentration gradient in SiO_x conforms to its spontaneous lithiation process, benefiting the electrochemical performance. These results highlight the focus on the working potential of carbon as a strategy for rational optimization of SiO_x/C composites toward improved battery performance.

Introduction

Silicon-based anode materials attract tremendous attention due to their huge theoretical capacity (3579 mAh g^{-1} for $Li_{15}Si_4$), nearly tenfold that of graphite (Gr, 372 mAh g^{-1} for LiC_6)[1, 2]. However, severe volume change effects, limited electronic and ionic conductivities, and continuous interfacial side reactions restrict their large-scale application[3, 4]. In recent years, researchers have turned their attention to silicon oxide, SiO_x ($0<x<2$)[5]. SiO_x inherits the high capacity of Si-based materials (2100 mAh g^{-1})[6], but suffers a less severe expansion/shrinkage during lithiation/delithiation, thus enabling an extended cycling life[7]. In addition, the lithium silicate (mainly Li_4SiO_4) and lithium oxide (Li_2O) in situ generated during the initial lithiation have positive effects on the mechanical stability and ionic conductivity of the material[8]. Despite this, a nonnegligible volume change effect remains the main limitation that prevents SiO_x to replace conventional Gr anodes[9, 10].

"Trapping effect" is prevalent in Si-based anodes[11-13], previous reports have mainly attributed this phenomenon to the limited electronic and ionic conductivity of Si-based materials, which inhibits the dealloying of Si-alloyed Li and thereby worsen the capacity performance. To enhance the conductivity as well as buffer the volume change, state-of-the-art SiO_x-based anodes combine SiO_x and Gr particles into composite materials[14-17]. However,

the intrinsic lithiation/delithiation potentials of SiO_x are significantly higher than those of Gr, which may induce a series of new problems[18].

The working potential vs. Li/Li^+ of a SiO_x anode is in the range 0-1 V (after activation), while that of Gr is generally below 0.2 V[19]. This working potential gap between the two materials prevents the simultaneous lithiation/delithiation of SiO_x and Gr within composite anodes, and it makes it sequential instead (being SiO_x the first in being lithiated and the latter in delithiation). Such inhomogeneous lithiation/delithiation leads to several complications, in which severe polarization of a single component is predictable. While such a drawback was already highlighted in some previous works on Si/Gr anode materials, e.g. in the works by Moon et al., Yao et al., and Son et al.[20-22], the exact mechanism behind the resulting instability and effective countermeasures to avoid it have not been provided and are therefore urgently sought after.

Pitch-derived soft carbon (SC) is a cheap industrial derivative whose internal microstructure is composed of randomly orientated Gr nanocrystals containing 3-4 graphitic layers[23]. This unique microstructure provides multiple paths for Li-ion migration, which provides SC with a characteristic sloping capacity profile[24]. Overall, the lithiation working potential of SC is higher than that of SiO_x, which means the implementation of SC can avoid the SiO_x prior lithiation in SiO_x/Gr (GrS). Therefore, the replacement of Gr by SC is expected to present a different electrochemical behavior. Practically, researchers have constructed Si/SC composite anodes for better performance[25, 26], but the gaps in the underlying electrochemistry of such composite electrodes demands filling. For this purpose, an insightful investigation of the electrochemical behavior of SiO_x/carbon (SiO_x/C) composites is needed to clarify the underlying mechanism of capacity decay and guide their optimization.

In this work, insights into the Li-ion storage behavior divergences and stress evolution of GrS and SiO_x/SC (SCS) anodes are provided. Also, the influence of the intrinsic working potential differences of SiO_x and carbon materials on these discrepancies is clarified. Using operando X-ray diffraction (XRD), we monitored the crystallographic evolution of the carbon component and quantitatively calibrated the real-time and simultaneous capacity contributions of SiO_x and carbon components. Additionally, finite element analyses were adopted to understand the Li-ion diffusion behaviors and related stress evolution driven by the concentration gradients at the contact surface of SiO_x and carbon. Overall, this work offers comprehensive knowledge of the Li-ion storage behaviors of SiO_x/C anodes, providing theoretical guidance for the optimization of SiO_x/C matching strategy toward future practical applications.

Results and Discussion

SC was obtained by the carbonization of the coal tar pitch precursor at 1600°C. Since the microstructure of a material greatly determines its electrochemical behavior, this was carefully analyzed for both Gr and Sc using high-resolution transmission electron microscopy (HRTEM). In contrast to the Gr sample presenting sharp parallel stripes and no visible grain boundaries (Fig. 1a), SC presents nanocrystalline domains of relatively curly and turbulent carbon layers (Fig. 1c). Selected area electron diffraction (SAED) patterns (insets of Fig. S1a, b) indicate that the graphitization degree of SC is relatively low. This result is confirmed by XRD patterns showing the SC sample to exhibit peaks with lower intensity and larger full width at half maximum than Gr (Fig. 1e). As measured by HRTEM and XRD via the Bragg equation ($n\lambda=2d\sin\theta$), SC presents significantly larger interlayer distances than Gr (Fig. S1a, b, and Table S1). The comparison of the lattice strain of the Gr and SC samples, as calculated by geometric phase analyses[27-29], indicates SC to present a strain distribution with a higher density and intensity, which will have associated a larger density of defects (Fig. 1b, d). Raman characterization showed the intensity ratio between the D band associated with disorder-induced vibration and the G band associated with the Gr E_{2g2} mode to be I_D/I_G = 0.80 for SC and I_D/I_G = 0.15 for Gr (Fig. 1f), confirming the much defective structure of SC[30]. Overall, the vast quantities of defect-rich grain boundaries, the expanded interlayer distance, and the small size of the randomly orientated crystal domains in SC can effectively ameliorate the intergranular and intragranular Li-ion diffusion kinetics, which will cause the SC to behave differently in electrochemistry[31].

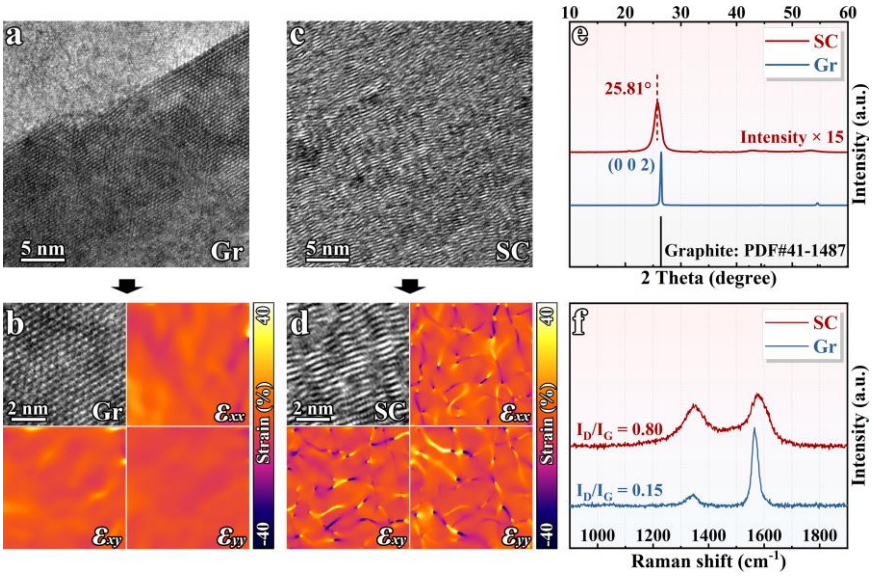

FIGURE 1 Structural characterization of Gr and SC samples. HRTEM images and strain distribution analyses of Gr (a, b) and SC (c, d) samples. (e) XRD patterns. (f) Raman spectra.

Generally speaking, due to the high oxygen content in SiO_x, irreversible lithiation products like lithium silicate and Li_2O form during the initial lithiation, reducing the initial coulombic efficiency (ICE). It has been reported that the metastable SiO_x can be disproportionated into two phases (Fig. S2a, b) via a proper heat treatment strategy[32, 33]: i) the Li-active Si nanodomains distributed in the amorphous SiO_2 matrix (Fig. S3), and ii) Li-reactionless SiO_2 matrix that can benefit ICE performance and capacity retention[34-36].

GrS and SCS composites were prepared by mixing disproportionated SiO_x with SC and Gr, respectively, at a mass ratio of 1:1 (see morphologies of micron-size SiO_x, Gr, and SC particles in Fig. S4-6). As references, the galvanostatic charge/discharge (GCD) profiles of the single-material electrodes (SiO_x, Gr, and SC) are depicted in Fig. S7a,b,d. The GrS and SCS composite electrodes inherit the major characteristics of SiO_x (Fig. S7c, e), indicating the domination of SiO_x component in the capacity contribution. Notably, the ICE of GrS and SCS are less affected by the type of carbon (Fig. S8), indicating that the process affecting the ICEs of the SiO_x/C electrodes may be associated with the SiO_x component and/or the interfacial side reaction between the two phases. In the normalized GCD profiles (Fig. 2a), the GCD curves of the SiO_x anode present a certain degree of hysteresis, which indicates that the SiO_x anode suffers from relatively high reaction energy barriers that induce sluggish lithiation/delithiation kinetics[37]. The dQ/dV curves of SiO_x, Gr, and SC anodes are displayed in Fig. 2b,c,e. The lithiation electrochemistry of SiO_x (active Si phase) presents two stages of electrochemical reactions, $Si \rightarrow Li_xSi_y$ (0.45-0.17 V) and $Li_xSi_y \rightarrow Li_{15}Si_4$ (0.17-0.01 V)[38, 39]. This is quite different from the lithiation behavior of Gr, which presents three main stages of phase transition of $Gr \rightarrow LiC_x$ (0.20 V), $LiC_x \rightarrow LiC_{12}$ (0.11 V), and $LiC_{12} \rightarrow LiC_6$ (0.07 V)[40]. Visibly, during the lithiation stage, the overall working potentials of Gr are below 0.20 V, significantly lower than those of SiO_x. Consistent with these differences, in the lithiation stage of GrS, a sequential lithiation is exhibited being SiO_x lithiated before Gr. In contrast, SC exhibits higher working potentials during delithiation with a relatively wide potential range (1.2-0 V), and the GCD curves present a sloping characteristic as expected. Thus, the dQ/dV profile of the corresponding SCS electrode (Fig. 2f) presents no significant variation compared with the SiO_x electrode (Fig. 2b). As for the delithiation stage, the working potential of Gr remains below that of SiO_x throughout, while that of SC partially overlaps with SiO_x. Due to the difference in carbon content, the lithiation/delithiation platforms of SCS and GrS present differences as well. Since the GrS anode exhibits working platforms below those of SCS, its lower working potential during

delithiation gives it a certain degree of increase toward the output voltage of the full-cell battery and improves the energy density (Fig. 2d,f). Despite this, a series of internal problems can be triggered by the intrinsic working potential difference between SiO_x and Gr that does more harm than good[41]. In view of this, it is crucial to disentangle the intrinsic electrochemical behavior mechanisms of GrS and SCS to understand how the SiO_x/C matching strategy influences the electrochemical performance of the electrode.

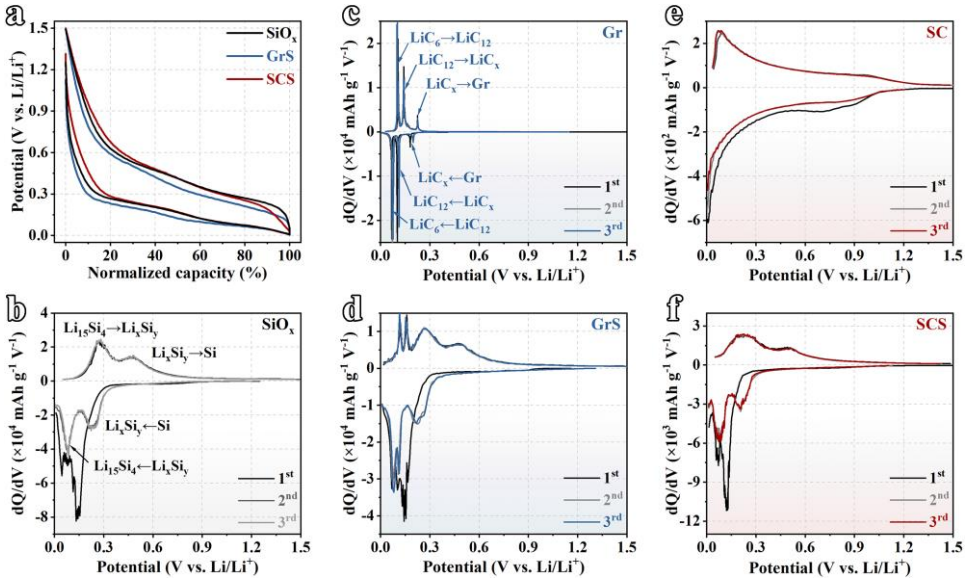

FIGURE 2 (a) Normalized GCD profiles of SiO_x, Gr, and SC electrodes. dQ/dV profiles of SiO_x (b), Gr (c), GrS (d), SC (e), and SCS (f) electrodes.

Operando XRD was used to quantify the capacity contribution of each component in the SiO_x/C anode at every lithiation/delithiation step. Because the Bragg reflection of SiO_x is relatively weak, particularly when the internal Si nanodomains transform to amorphous after lithiation/delithiation, we aimed at tracking the (0 0 2) plane evolutions of the Gr and SC components to understand the Li-ion storage behaviors in GrS and SCS electrodes. First, the single-phase reference calibration of the carbon components is required. As depicted in Fig. 3a, Gr exhibits the Bragg reflections of various graphite intercalation compounds (GICs) with different Li/C atomic ratios in the lithiation stage. With the gradual deepening of the intercalation process, the amount of Li between Gr layers gradually accumulates, and the interlayer between (0 0 2) planes expand accordingly. Given the phase evolution of GICs, five main stages can be defined: Stage 1) Gr interlayer expansion with a small amount of Li embedded; Stage 2) GICs with low Li content are formed; Stage 3) GICs transform to LiC_{12} phase; Stage 4) phase transition from LiC_{12} to LiC_6; and Stage 5) the crystallization degree of LiC_6 increases[42]. As for the delithiation process, Gr presents an almost symmetric phase

evolution from LiC_6 to LiC_{12}, and finally to Gr phase through a series of intermediate GICs with different atomic ratios[43].

When it comes to the SC anode, things become even more interesting. The (0 0 2) Bragg reflection continuously shifts to lower/higher angles during the lithiation/delithiation of SC (Fig. 3b). Since SC is a polycrystalline material composed of a large number of nanocrystals with different orientations, Li-ions can take the innumerable available migration paths during the lithiation/delithiation. The parallel availability of such countless possibilities for Li-ion diffusion decreases the resistance against Li-ion diffusion between and inside the nanocrystals. With the gradual deepening of the lithiation degree, the (0 0 2) Bragg reflection finally reaches the characteristic 2theta value of LiC_6, which indicates that in the fully lithiated state, the SC nanocrystals possess the same crystal structure as the fully lithiated Gr.

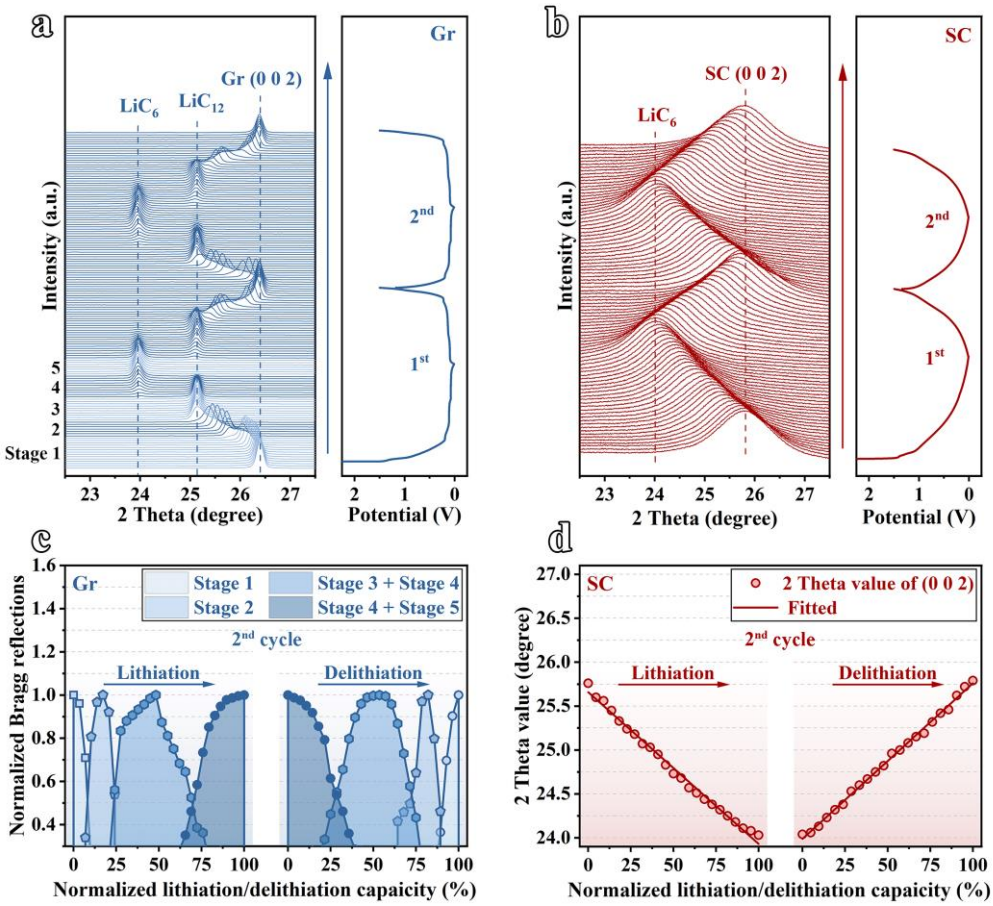

FIGURE 3 Operando XRD patterns of 2 cycles at 0.1C of Gr (a) and SC (b) electrodes. The constructed relationships between instantaneous capacity and Bragg reflection during the 2nd cycle of Gr (c) and SC (d) electrodes.

Based on the comparison of operando XRD and GCD profiles, the relationships between capacities and Bragg characteristics can be constructed (2nd cycle, Fig. 3c, d). Fig. 4a and b

depict the contour map operando XRD patterns of Gr and GrS electrodes, and Fig. 4c and d displays those of SC and SCS (the raw data of GrS and SCS is plotted in Fig. S10a, b). In the case of Gr, each instantaneous capacity is featured with a unique characteristic Bragg reflection intensity (areal integral) in the corresponding stage. After normalizing the Bragg reflection intensities of each stage, the relationship between capacity and the operando (0 0 2) plane evolution of Gr can be obtained. As for SC, things are even simpler. Thanks to the almost linear relationship between the capacity and characteristic 2theta value of (0 0 2) plane, a fitted linear relationship can be obtained associated with each instantaneous capacity.

The crystallographic evolutions of Gr and SC single-phases are inherited in the GrS and SCS composites. However, the intrinsic work potential gaps between Gr, SC, and SiO_x play an important role. Since Gr has a lower lithiation potential than SiO_x, within the GrS electrode, Stages 1 and 2 of Gr lithiation are extended over a relatively long period of time and the formation of GIC in GrS electrode is significantly delayed when compared with the evolution observed in Gr electrode. On the other hand, the transition from LiC_{12} to LiC_6, which occupies nearly 50% of the capacity of Gr, takes place in a much shorter period of time in the GrS electrode, and the LiC_6 crystallization is not completed (Fig. S11). This shorter time for the GIC transition is related to the fact that, within GrS, the potential is determined by the SiO_x component which is the one dominating the capacity contribution. Since the lithiation potential of SiO_x is higher than that of Gr, in the last period of GrS lithiation, SiO_x fastly goes across the potential range of $LiC_{12} \rightarrow LiC_6$, which leads to the Stages 3-5 being shortened.

Under such circumstances, the actual allocated current density on each component (especially Gr at Stages 3 to 5) is even larger because the lithiation flows only through part of the material (SiO_x initially), thus the internal polarization effect is more severe than expected. Consequently, the fully lithiated GrS electrode presents a lower crystallization degree of LiC_6 than in the Gr electrode (Fig. S11), inducing a partial loss of the terminal capacity contribution of Gr in GrS. Meanwhile, at the early stage of the lithiation, the almost single-phase lithiation (SiO_x) will induce a much higher Li concentration on SiO_x particles than on the adjacent Gr particles, resulting in a reverse diffusion of Li-ions, i.e. from SiO_x towards Gr. Since the lithiation of SiO_x is generally an outside-in process, that is, Li-ions migrate from the surface to the core, the opposite diffusion behaviors are bound to harm the SiO_x capacity.

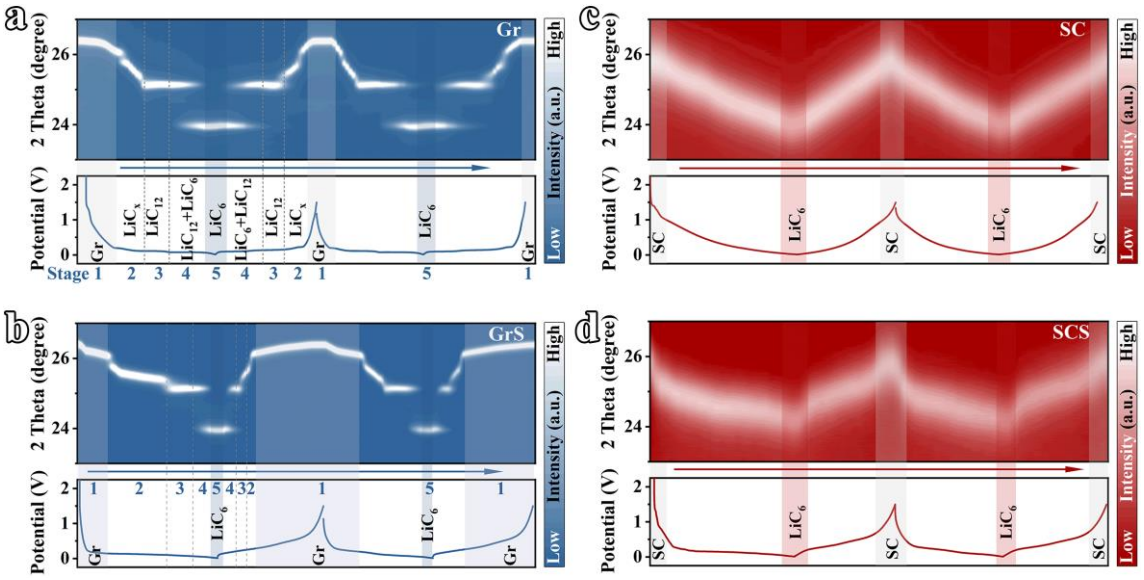

FIGURE 4 Contour map operando XRD patterns of 2 cycles for Gr (a), GrS (b), SC (c), and SCS (d) electrodes.

The capacity contribution of GrS can be calibrated via the construction of a matrix polynomial (equation 1, see parameter definitions in Fig. S9 and Table S2). Similarly, a matrix polynomial for SCS was constructed (equation 2, see parameter definitions in Table S3). In the capacity contribution calibration of GrS (Fig. 5a), unexpectedly, the capacity contribution of SiO_x presents an even decrease on the route of lithiation, which provides evidence for the bidirectional diffusion phenomenon on the surface of SiO_x. Unlike the GrS electrode, because the intrinsic lithiation potential of SC is higher than that of SiO_x, the SCS electrode quickly goes through the earlier Li-poor stage of SC (Fig. 5b), and slowly goes through the subsequent Li-rich stage until the complete lithiation to LiC_6. Since the SC component possesses higher lithiation potential than SiO_x, the concentration gradient of Li-ions at the interface directs from SC to SiO_x during lithiation, which is consistent with the inner Li diffusion direction in SiO_x during lithiation, thus the negative effects caused by the bidirectional diffusion in GrS is avoided. Moreover, SC possesses higher Li-ion diffusion kinetics compared with Gr, facilitating the performing of the high-capacity advantage of SiO_x component.

$$\begin{bmatrix} I_{Stage\ n_a} \\ \vdots \\ I_{Stage\ n_z} \end{bmatrix}^T \begin{bmatrix} k_{Stage\ n_a} \\ \vdots \\ k_{Stage\ n_z} \end{bmatrix} + \begin{bmatrix} C_{SiO_{x\_a}} \\ \vdots \\ C_{SiO_{x\_z}} \end{bmatrix} = \begin{bmatrix} C_{Stage\ n_a} \\ \vdots \\ C_{Stage\ n_z} \end{bmatrix} \quad (1)$$

$$\begin{bmatrix} d_{SC_a} \\ \vdots \\ d_{SC_z} \end{bmatrix}^T \begin{bmatrix} f_{SC_a} \\ \vdots \\ f_{SC_z} \end{bmatrix} + \begin{bmatrix} C_{SiO_{x\_a}} \\ \vdots \\ C_{SiO_{x\_z}} \end{bmatrix} = \begin{bmatrix} C_a \\ \vdots \\ C_z \end{bmatrix} \quad (2)$$

To simulate the Li concentration evolution behavior in the bulk phase of the electrode materials during the lithiation process, finite element analyses were used. Since physicochemical diffusion behaviors follow Fick's second law[44, 45], by equating the Li concentration diffusion to temperature variation, the heat conduction module can be adopted to realize Li-ion diffusion analyses. Fig. 5c shows the system before Gr induces a concentration gradient of Li-ions directed from SiO_x to the adjacent Gr at the contact interface. As the lithiation degree of the electrode increases, the potential gradually decreases to the lithiation potential of Gr (0.2 V vs. Li/Li^+), when the adjacent Li-ion is captured by Gr under the dual drive of potential and concentration gradient. Fig. 5d shows the situation when the Li-ion in the outer layer of SiO_x is captured by Gr due to the concentration gradient. On one hand, the lithiation of SiO_x is controlled by the diffusion of Li in the bulk phase, during which a Li concentration gradient is generated from the outside to the inside. On the other hand, the capture of Li-ion in the outer surface layer of SiO_x by Gr will induce a lower ionic concentration on the surface than in the subsurface, thereby resulting in a bidirectional diffusion (Fig. 5e). In the meantime, given that the lithiation and delithiation are always accompanied by volume expansion and contraction, the escape of the superficial Li will lead to the contraction of the SiO_x outer layer and cause an inward compressive stress, inhibiting subsequent lithiation. This bidirectional diffusion behavior is one of the important reasons why micron-size SiO_x/Gr composites generally fail to reach the expected performance. In contrast, as the working potential of SC is higher than SiO_x in SCS, SC experiences a prior lithiation in advance (Fig. 5f). During this period, the higher concentration of Li in SC leads to the formation at the interface of a concentration gradient towards SiO_x, and the Li-ion in the superficial layer of SC will be captured by SiO_x. However, considering the relatively high ionic conductivity and the almost negligible volume effect of SC, such Li-ion migration behavior will have scarcely any negative impact on the capacity of SC. In terms of SiO_x, the lithiation process itself is an inward diffusion process from the outer layer, which is in the same direction as the interfacial concentration gradient driving Li migration (Fig. 5g). The diffusion processes of GrS and SCS in 2D perspective are present in Fig. S12, 13.

To further confirm the above conjecture, at the 50^{th} and 100^{th} cycles of the GrS electrode, the lithiation temperature was set to 85°C (electrolyte and Li foil renewed after the exceptional lithiation) to fully promote the internal Li-ion diffusion and eliminate polarization. As expected, the reversible capacity of the GrS electrode almost recovers to an equal capacity to that of the SCS electrode but rapidly decays in the subsequent cycles again (Fig. 5h). This phenomenon provides further evidence for the above explanations.

As for the delithiation process, the working potential of Gr is lower than SiO_x, while that of SC presents a lower-to-higher characteristic than SiO_x. In the early stage of delithiation, both Gr and SC experience prior delithiation. At this time, the concentration gradient at the interface of GrS and SCS induces the capture of Li-ion by Gr and SC, during which the surface of SiO_x will shrink, and the resulting compressive stress can promote the further delithiation of the SiO_x core[46]. This process is likewise orthokinetic with the delithiation behavior of SiO_x itself in both GrS and SCS. However, the polarization effect of a single component in SCS is bound to be smaller due to the certain degree of overlap working potentials of SC and SiO_x during delithiation.

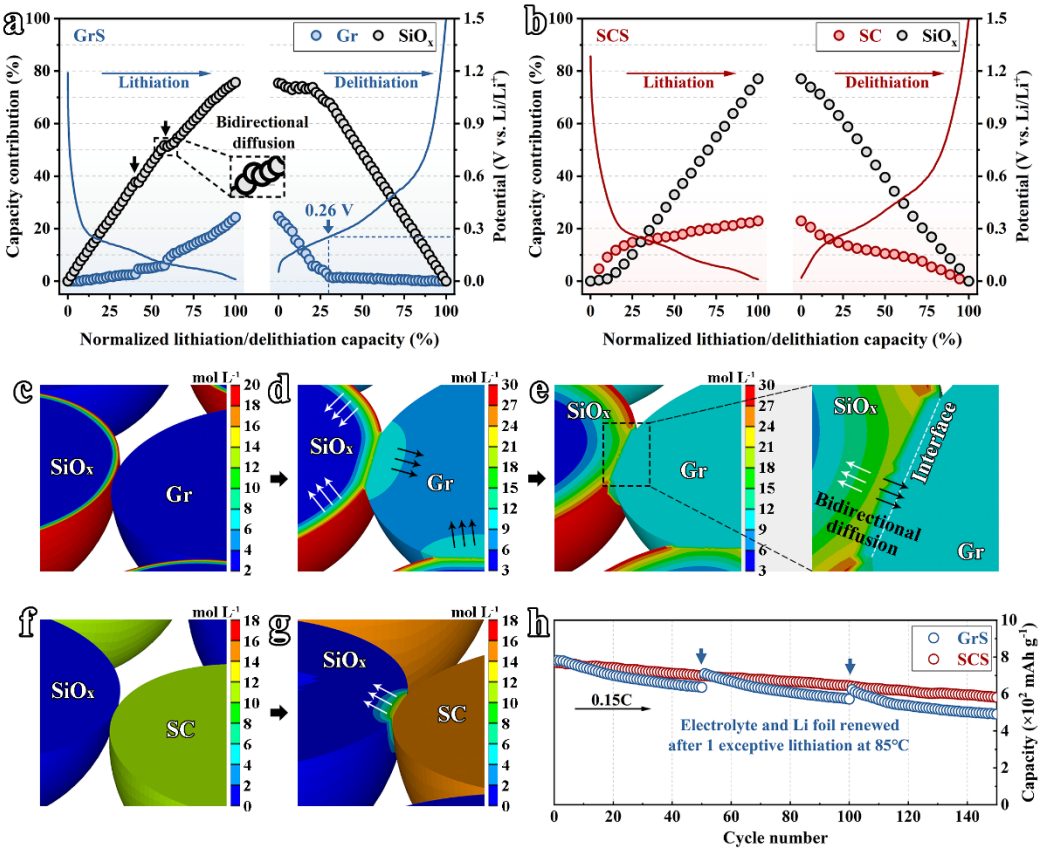

FIGURE 5 Capacity contribution calibrations for GrS (a) and SCS (b) electrodes. Finite element simulation results of Li-ion concentration distributions and diffusion behaviors during lithiation for GrS (c-e) and SCS (f, g) electrodes. (h) Cycling performances of GrS and SCS (electrolyte and Li foil renewed at 50th and 100th cycle after exceptive lithiation at 85°C) electrodes.

Conclusion

In summary, since the intrinsic working potential of Gr is lower than SiO_x, the lithiation/delithiation process of each component in GrS tends to perform sequentially rather

than simultaneously. This Li-ion storage behavior inevitably leads to a bidirectional Li diffusion phenomenon at the SiO_x surface as well as to the polarization of a single component, which cause the shrinking of the SiO_x surface lattice blocking additional lithiation. For SCS electrodes, as the SC itself has a higher working potential than SiO_x, the SC is priorly lithiated. The concentration gradient at the interface between SC and SiO_x does not result in Li diffusion inhibition during the lithiation of SiO_x. Consequently, the constraint on further lithiation led by superficial compressive stress of the SiO_x can be avoided, thus allowing taking full advantage of the high-capacity of the SiO_x material. Nevertheless, it cannot be neglected that within the SiO_x/C composite, SC still suffers from the disadvantages of inadequate ICE and relatively low reversible capacity. Regarding the carbon component, the key point to optimize the matching of SiO_x/C is realizing the appropriate lithiation working potential of carbon via the regulation of the internal microstructure, while the modification of its ICE and improvement of its capacity are also important factors. Overall, the optimized matching of the lithiation/delithiation of carbon materials and SiO_x is bound to realize superior electrochemical performance.

Methods

Raw Materials. Micron-size SiO_x powder was purchased from Aladdin Co., Ltd. (Shanghai, China). Artificial graphite (Gr) powder and coal tar pitch were supplied by Shenzhen Solid Advanced Materials Technology Co., Ltd. (Shenzhen, China).

Modifications and Syntheses of Materials. SiO_x disproportion: SiO_x powder with an average particle size of about 7 μm was placed in a quartz boat and heated in a tubular furnace at a rate of 10°C min^{-1} (Ar atmosphere). After being preserved at 1000°C for 1h, the furnace was cooled down and disproportionated SiO_x material is finally obtained[38]. Soft carbon (SC) preparation: Coal tar pitch in a corundum crucible was placed in the tube furnace and heated with a N_2 atmosphere and a heating rate of 10°C min^{-1}. After being preserved at 1000°C for 2h, the material was heated up to 1600°C and carbonization for 3h[47]. After cooling down, the SC product was fully ground to micron size.

Characterization techniques. SEM: JEOL JEM-7600F (15 kV). TEM: JEOL JEM-2100F (200 kV). XRD: Rigaku Miniflex 600 (40 kV, 15 mA, Cu Kα, 5° min^{-1}). Raman spectra: Renishaw Invia Reflex (532 nm laser).

Operando XRD Characterization. The operando XRD characterizations were performed based on a Rigaku Miniflex 600 (40 kV, 15 mA, Cu Kα, 5° min^{-1}). Typically, a stainless-steel mold was used as the battery shell, the insulating area was achieved by a polyimide film, and the upper side window adopted Be metal foil to assemble the operando battery. Particularly,

considering the low Bragg signal intensity of SC, the operando XRD patterns of the SC electrode were acquired at a relatively lower sweep speed. Glass fiber membrane (Whatman GF/C) was used as the separator to avoid the interplay of the Bragg reflections from the Li metal counter electrode during the collection of the operando XRD profiles[39].

Batteries. Electrode: The electrode slurry was prepared according to a mass ratio of 8:1:1 (active materials: Super P: binder), and was magnetically stirred in pure water solvent. Then the slurry was evenly coated on the copper foil and dried in a vacuum drying oven at 100°C for 12h. Afterward, the fully-dried electrode was punched into circles with a diameter of 16 mm.

Battery assembly: 2032-coin cells were assembled in a glove box (H_2O<1 ppm, O_2<1 ppm). Li metal foil was used as the counter electrode and Celgard 2000 as the separator. The electrolyte contains 1.0 M $LiPF_6$ dissolved in an EC: DEC: FEC=3:7:1 (volume ratio) solvent for better SEI formation[21]. After the battery was assembled, a 12h standing treatment was performed before the test to guarantee the complete wetting of the electrolyte towards the electrode. Electrochemical test: Constant current charge-discharge (GCD) tests were performed on Land CT2001A. dQ/dV profiles were derived from the GCD profiles.

Finite element simulations. For the common physicochemical diffusion behaviors, the diffusion concentration of a substance changes with time, which is an unsteady diffusion process. The process follows Fick's second law[48]:

$$\frac{\partial C}{\partial t}=D\frac{\partial^2 C}{\partial x^2} \tag{1}$$

The ionic diffusion equation can be obtained from Fick's second law[49]:

$$\frac{\partial C}{\partial t}=\frac{\partial}{\partial x_i}D_{ij}\left(\frac{\partial C}{\partial x_j}\right) \tag{2}$$

Equation (2) is expanded as follows:

$$\frac{\partial C}{\partial t}=\frac{\partial}{\partial x}\left(D_{xx}\frac{\partial C}{\partial x}\right)+\frac{\partial}{\partial y}\left(D_{yy}\frac{\partial C}{\partial y}\right)+\frac{\partial}{\partial z}\left(D_{zz}\frac{\partial C}{\partial z}\right) \tag{3}$$

Considering that the interior of the material is generally isotropic, it is defined that $D_{xx}=D_{yy}=D_{zz}=D$, the equation can be simplified as follows[50]:

$$\frac{\partial C}{\partial t}=D\left(\frac{\partial^2 C}{\partial x^2}+\frac{\partial^2 C}{\partial y^2}+\frac{\partial^2 C}{\partial z^2}\right) \tag{4}$$

By equivalenting the concentration diffusion of lithium to temperature diffusion, the Li-ion diffusion analyses in the finite element software ANSYS are realized via carrying out the heat conduction module[51]. However, it should not be ignored that different from the process of heat conduction, the temperature in the process of heat conduction presents continuous changes,

while the change of Li-ion concentration in the interface between different electrode materials is not continuous, especially when considering theoretical capacity differences of various electrode materials led saturated concentration differences, which limits the use of finite element analyses to simulate the ionic diffusion behaviors. In view of this, using relative concentration (*w*, Table S4), namely to local Li-ion concentration with the corresponding saturated Li-ion concentration ratios to substitute local concentration, such treatment can make the field variables keep continuous at the interface of electrode materials. The temperature variable is defined as the concentration variable, where the highest concentration is 1 and the lowest concentration is 0. The diffusion coefficients of SiO_x[52], Gr[53], and SC are given by reported works[54]. Simulation for GrS: The initial state is the SiO_x sphere contacts with Gr sphere and only the relative concentration of SiO_x is given 1. Since the lithiation potential of SiO_x is higher than that of Gr, the SiO_x will be lithiated priorly, and the lithium in the SiO_x particle will diffuse to Gr. In this case, the model is set as that there is a certain surface contact between the two, and the relative concentration of the contact surface is still 1 (due to the higher ionic conductivity of the Gr interior, the Li-ion concentration of the Gr outer layer has not been reassigned thereafter). Simulation for SCS: The initial state defaults to the contact of two spherical particles (SiO_x and SC) and only the relative concentration of SC is given 1. When the SC is priorly lithiated due to its higher working potential than SiO_x, the Li-ion in SC will diffuse to SiO_x. At this time, no concentration value is assigned to the contact surface, nor to SiO_x, and it relies on free diffusion behavior.

Data availability

All data will be made available on request.

Declaration of Competing Interest

The authors declare that they have no known competing financial interests or personal relationships that could have appeared to influence the work reported in this paper.

Acknowledgements

Q.S. and G.Z. contributed equally to this work. This work was supported by the School Research Startup Expenses of Harbin Institute of Technology (Shenzhen) (DD29100027), the High-level Talents' Discipline Construction Fund of Shandong University (31370089963078), the National Natural Science Foundation of China (52175300, 52105329), and the project NANOGEN (PID2020-116093RB-C43) funded by MCIN/ AEI/10.13039/501100011033/.

ICN2 acknowledges funding from Generalitat de Catalunya 2017 SGR 327, the Severo Ochoa program from Spanish MCIN / AEI (CEX2021-001214-S), and the CERCA Programme / Generalitat de Catalunya. This work was supported by MCIN with funding from European Union NextGenerationEU (PRTR-C17.I1) and Generalitat de Catalunya. Part of the present work has been performed in the framework of Universitat Autònoma de Barcelona Materials Science PhD program. G.Z. thanks the China Scholarship Council for the scholarship support.

Appendix A. Supplementary material

Supplementary data to this article can be found online at http://doi.org/xxxxxxx

References

[1] Y. Cui, Nature Energy, 6 (2021) 995-996.
[2] K. Turcheniuk et al., Materials Today, 42 (2021) 57-72.
[3] R.F.H. Hernandha et al., Advanced Functional Materials, 31 (2021) 2104135.
[4] D. Martín-Yerga et al., Angewandte Chemie International Edition, 61 (2022) e202207184.
[5] A. Hirata et al., Nature communications, 7 (2016) 11591.
[6] H. Yamamura et al., Journal of the Ceramic Society of Japan, 119 (2011) 855-860.
[7] J. Sung et al., Nature Energy, 6 (2021) 1164-1175.
[8] Z. Liu et al., Chemical Society Reviews, 48 (2019) 285-309.
[9] D.J. Chung et al., Small, 18 (2022) 2202209.
[10] Y.-F. Tian et al., Advanced materials, 34 (2022) 2200672.
[11] D. Rehnlund, Z. Wang, L. Nyholm, Advanced materials, 34 (2022) 2108827.
[12] Q. Ai et al., Advanced Materials Interfaces, 6 (2019) 1901187.
[13] B. Zhu et al., Science Advances, 5 (2019) eaax0651.
[14] P. Li, J.-Y. Hwang, Y.-K. Sun, ACS nano, 13 (2019) 2624-2633.
[15] X.-D. Li et al., ACS applied materials & interfaces, 14 (2022) 27854-27860.
[16] K. Kierzek, J. Machnikowski, F. Béguin, Journal of Applied Electrochemistry, 45 (2015) 1-10.
[17] L. Li et al., ACS Applied Energy Materials, 4 (2021) 8488-8495.
[18] Z. Zhao et al., Batteries & Supercaps, 2 (2019) 1007-1015.
[19] J. Park, S.S. Park, Y.S. Won, Electrochimica Acta, 107 (2013) 467-472.
[20] J. Moon et al., Nature communications, 12 (2021) 2714.
[21] K.P.C. Yao et al., Advanced Energy Materials, 9 (2019) 1803380.
[22] S.-B. Son et al., Advanced Science, 6 (2019) 1801007.
[23] Y.-N. Jo et al., Electrochimica Acta, 146 (2014) 630-637.
[24] N.N. Sinha et al., Journal of The Electrochemical Society, 159 (2012) A1672.
[25] N. Kobayashi, Y. Inden, M. Endo, Journal of Power Sources, 326 (2016) 235-241.
[26] Y. He et al., Electrochimica Acta, 373 (2021) 137924.
[27] M.J. Hÿtch, E. Snoeck, R. Kilaas, Ultramicroscopy, 74 (1998) 131-146.
[28] S.G. Kwon et al., Nature Materials, 14 (2015) 215-223.
[29] R. Zhang et al., Physical Review B, 59 (1999) R6585-R6588.
[31] H. Azuma, H. Imoto, S.i. Yamada, K. Sekai, Journal of Power Sources, 81-82 (1999) 1-7.
[32] X. Bi et al., Small, 18 (2022) 2200796.
[33] J. Guo et al., Electrochimica Acta, 342 (2020) 136068.
[34] J. Wang et al., Nano Energy, 78 (2020) 105101.
[35] J. Li et al., Energy & Fuels, 35 (2021) 16202-16211.
[36] J.-I. Lee et al., Angewandte Chemie International Edition, 51 (2012) 2767-2771.
[37] A. Ostadhossein et al., The Journal of Physical Chemistry A, 120 (2016) 2114-2127.
[38] K. Kitada et al., Journal of the American Chemical Society, 141 (2019) 7014-7027.
[39] Q. Sun et al., ACS applied materials & interfaces, 14 (2022) 14284-14292.
[40] J. Zhou et al., Small, 18 (2022) 2107460.
[41] X. Gao, J. Xu, Journal of Electrochemical Energy Conversion and Storage, 19 (2022) 041004.
[42] H. Fujimoto et al., Journal of The Electrochemical Society, 168 (2021) 040509.

[43] L. Xu et al., Small, 18 (2022) 2105897.
[44] V. Zadin et al., Solid State Ionics, 192 (2011) 279-283.
[45] V. Ramadesigan et al., Journal of The Electrochemical Society, 157 (2010) A854.
[46] V.A. Sethuraman et al., Journal of The Electrochemical Society, 157 (2010) A1253.
[47] Y. Liu et al., Advanced materials, 32 (2020) 2000505.
[48] S. Ding, W.T. Petuskey, Solid State Ionics, 109 (1998) 101-110.
[49] A.A.O. Tay, L. Tingyu, IEEE Transactions on Components, Packaging, and Manufacturing Technology: Part A, 19 (1996) 186-193.
[50] K. Nicolay et al., NMR in Biomedicine, 14 (2001) 94-111.
[51] X.H. Liu et al., ACS nano, 6 (2012) 1522-1531.
[52] W. Xu et al., Small Science, 2 (2022) 2100105.
[53] P. Yu et al., Journal of The Electrochemical Society, 146 (1999) 8.
[54] H.-j. Guo et al., New Carbon Materials, 22 (2007) 7-10.

Declaration of interests

☒ The authors declare that they have no known competing financial interests or personal relationships that could have appeared to influence the work reported in this paper.

☐The authors declare the following financial interests/personal relationships which may be considered as potential competing interests: